



Cite this: *Org. Biomol. Chem.*, 2022, **20**, 2392

Received 27th January 2022,
Accepted 8th February 2022

DOI: 10.1039/d2ob00177b

rsc.li/obc

Atropselective synthesis of *N*-aryl pyridones via dynamic kinetic resolution enabled by non-covalent interactions†

Jamie S. Sweet, Ruichen Wang, Panagiotis Manesiotis, Paul Dingwall and Peter C. Knipe*

The dynamic kinetic resolution of C–N atropisomeric pyridones was achieved via asymmetric phase-transfer catalysis, exploiting a rotational barrier-lowering hydrogen bond in the starting materials. X-ray and NMR experiments revealed the presence of a barrier-raising ground state CH $\cdots\pi$ interaction in the product, supported by DFT calculations. A co-crystal of the quinidine-derived phase-transfer catalyst and substrate reveals key substrate–catalyst non-covalent interactions.

Chiral atropisomeric C–N axes have gained increasing interest, not least due to bioactive compounds such as sotorasib, a first-in-class KRAS inhibitor for the treatment of non-small-cell lung cancer (Fig. 1A). Axially chiral acetanilides also comprise a class of potent herbicides including metolachlor and dimethenamid. The asymmetric synthesis of such molecules has therefore been the subject of synthetic efforts.¹ Recent catalytic strategies include proximal C–N bond formation (where the C–N bond formed is not the axial bond),² *ortho*-CH functionalisation,³ desymmetrisation by remote functionalization,⁴ *de novo* pyridone synthesis by cycloaddition,⁵ and direct, intermolecular axial amination (Fig. 1B).⁶ During a research programme directed at synthesizing *N*-arylpyridinium and quinolinium salts⁷ we became interested in the atropselective synthesis of 2-pyridones. We were intrigued by reports by Smith, Paton *et al.*⁸ that phase-transfer catalysed (PTC) dynamic kinetic resolution (DKR) formed axially chiral benzamides, enabled by a transition state-lowering hydrogen bond in the phenol substrates (Fig. 1C).⁹ This approach has never been applied to axially chiral 2-pyridones.¹⁰ *A priori* it was unclear if the rotational barrier in an *N*-aryl pyridone starting

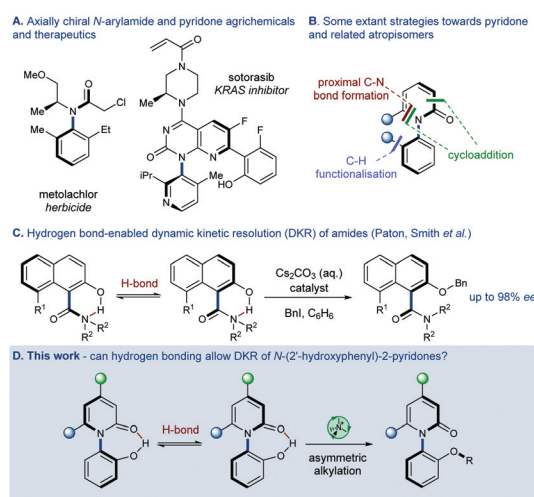


Fig. 1 Background to this study.

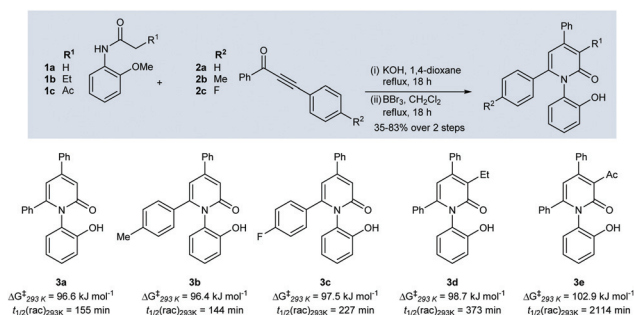
material would be sufficiently low to allow a DKR to be achieved, rather than a kinetic resolution. However, we reasoned that the ability of the starting material to form a 7-membered OH \cdots O hydrogen bond may reduce its rotational barrier compared with an alkylated product enabling DKR (Fig. 1D).

The rotational barriers of these compounds (generated from anisidine derivatives **1a–c** and 1,3-diarylpropynones **2a–2c** according to the method of Tang, Pan *et al.*¹¹) were measured experimentally (Scheme 1). Values for **3a–3c** were similar in magnitude, while 3-ethyl **3d** had a slightly higher barrier and 3-acetylated pyridone **3e** had this a significantly higher value. These barriers and the corresponding racemisation half-lives demonstrated that a DKR may be possible in a reaction lasting several hours. Early screening showed cinchonidinium catalyst **C1** to generate benzylated product **4a** in 66% ee (Table 1). Use of benzyl iodide in place of bromide (entry 2) gave a small increase in ee to 73%. *O*-Allyl catalyst **C2** significantly decreased enantioselectivity (entry 3), suggesting hydrogen bonding to the alcohol is important. Quinine-derived cata-

School of Chemistry and Chemical Engineering, Queen's University Belfast, David Keir Building, Belfast, BT9 5AG, UK. E-mail: p.knipe@qub.ac.uk; <http://www.knipechem.co.uk>

† Electronic supplementary information (ESI) available. DFT data relating to this study can be found at <https://pure.qub.ac.uk> with DOI: 10.17034/57c858bd-52ab-46c7-ac95-594e1fb66542. CCDC 2124143 and 2124208–2124211. For ESI and crystallographic data in CIF or other electronic format see DOI: 10.1039/d2ob00177b





Scheme 1 Synthesis of 2'-hydroxyphenyl-2-pyridone substrates. Rotational barriers (in kJ mol^{-1}) were determined by thermal racemization analysis on enantiopure samples obtained by analytical HPLC on a chiral stationary phase.

Table 1 Selected optimization data for enantioselective dynamic kinetic resolution (see ESI† for full screening)^a

Entry	Catalyst	Bn-X (eq.)	T (°C)	Approx. conv. ^b (%)	ee ^c (%)
1	C1	BnBr (0.6)	rt	<25	-66
2	C1	BnI (0.6)	rt	<25	-73
3	C2	BnI (0.6)	rt	<25	-33
4	C3	BnI (5)	rt	<25	-76
5	C4	BnI (5)	rt	<25	85
6	C4	BnI (5)	35	50–75	80

^a Reactions conducted on 41 μmol scale in CHCl_3 . ^b Conversion approximated by visual inspection of TLC plates and divided into the categories: <25%, 25–50%, 50–75%, >75%. ^c Determined by HPLC on a chiral stationary phase.

lyst C3 gave a slight increase in ee relative to C1 that lacks the quinoline methoxy substituent, and its *pseudo*-enantiomer C4 gave the opposite enantiomeric product in 85% ee (entry 5). The conversion under these conditions was low, so to make the reaction a practical synthetic method the temperature was increased to 35 °C, with the drop in ee to 80% a necessary but acceptable compromise (entry 6).

The scope of the asymmetric reaction was then explored (Table 2). Treatment of **3a–e** with benzyl iodide gave products **4a,d,g,j,m** in generally good yields but with a wide range of ees. Those lacking substitution at the pyridone 3-position generally gave higher ee, (65–77%), while the 3-ethyl product **4j** gave a much lower 40% ee, and 3-acetyl compound **4m** was obtained with a meagre 6% ee. This pattern, wherein substitution at the pyridone 3-position is poorly tolerated, was further borne out in reaction with electron-deficient and electron-rich benzylating agents. Lastly, alkylation with prenyl bromide gave the product **4p** with 47% ee, slightly lower than the benzylated products derived from the same phenol **4g–i**. The rotational barriers of the products were measured and dis-

Table 2 Substrate scope and limitations of dynamic kinetic resolution^a

Product	R ¹	R ²	R ³	Yield ^b (%)	ee ^c (%)	$\Delta G^{\ddagger}_{353\text{K}}$ ^d (kJ mol^{-1})
4a	Bn	C ₆ H ₅	H	77	75	121.3
4b	<i>p</i> -CNBn	C ₆ H ₅	H	80	67	122.3
4c	4-MeBn	C ₆ H ₅	H	76	70	122.1
4d	Bn	<i>p</i> -C ₆ H ₄ CH ₃	H	70	77	121.8
4e	4-CNBN	<i>p</i> -C ₆ H ₄ CH ₃	H	86	67	122.2
4f	4-MeBn	<i>p</i> -C ₆ H ₄ CH ₃	H	66	60	122.7
4g	Bn	<i>p</i> -C ₆ H ₄ F	H	70	65	122.7
4h	4-CNBN	<i>p</i> -C ₆ H ₄ F	H	86	58	122.3
4i	4-MeBn	<i>p</i> -C ₆ H ₄ F	H	63	51	122.5
4j	Bn	C ₆ H ₅	Et	53	40	121.0
4k	4-CNBN	C ₆ H ₅	Et	70	28	120.6
4l	4-MeBn	C ₆ H ₅	Et	33	41	120.4
4m	Bn	C ₆ H ₅	Ac	66	6	122.6
4n	4-CNBN	C ₆ H ₅	Ac	69	3	N.D. ^e
4o	4-MeBn	C ₆ H ₅	Ac	54	5	121.7
4p	Prenyl	<i>p</i> -C ₆ H ₄ F	H	79	47	121.5

^a Typical procedure: 2-pyridone (0.3 mmol), benzyl iodide (5 eq.), catalyst C4 (15 mol%), CHCl_3 (11 mL), K_2CO_3 (50% aq., 205 μL , 5 eq.), 35 °C, 42 h. ^b Yields are for isolated material. ^c Enantiomeric excesses determined by HPLC on a chiral stationary phase with reference to a racemic standard. ^d Rotational barriers determined by HPLC sampling from a DMSO solution held at 353 K. ^e Not determined since low ee of material made experimental error in measurement unacceptably high.

played only minimal variation across the products formed. The barriers of the products are approximately 25 kJ mol^{-1} higher than the phenol starting materials, supporting the hypothesis that the absence of the hydrogen bond donor leads to an increased transition state energy in the products. Eyring analysis also allowed the room temperature racemization half-lives of the products to be estimated as >1.6 years (see ESI†).

The intolerance of the reaction to substitution at the pyridone 3-position merits discussion. Substitution at this position increases rotational barriers in the starting materials (see Scheme 1). The reasons for this are primarily steric buttressing for the 3-ethyl compounds,¹² but may also have an electronic component for **3e**, where the acetyl group's electron-withdrawing effect may reduce the basicity of the lactam carbonyl, leading to a weaker (and less stabilising) hydrogen bond in the enantiomerisation transition state. Substitution at the 3-position may therefore impact the enantioselectivity through: (i) steric clashing with catalyst C4 that prevents tight binding when the 3-position is substituted; (ii) the increased barrier to rotation may cause **3d** and **3e** to operate partially or fully in a KR regime, rather than DKR; and (iii) tight catalyst binding may require rotation around the axis in an induced fit manner, so when the barrier is high, catalyst-substrate binding becomes less energetically favourable.

Single crystal X-ray diffraction of (+)-**4b** allowed assignment of the major enantiomeric product, and to examine the struc-



ture and conformation of the products alongside racemic crystals of **4a**, **4j** and **4m** (Fig. 2A). The absolute stereochemistry of **4b** is (*R_a*), and we assume by extension that the (*R_a*)-atropisomer is favoured in all products. An unexpected tilt was observed in the crystal structures of all products (θ), with values ranging from 10.3° (**4b**) to 15.6° (**4m**). The cause of this

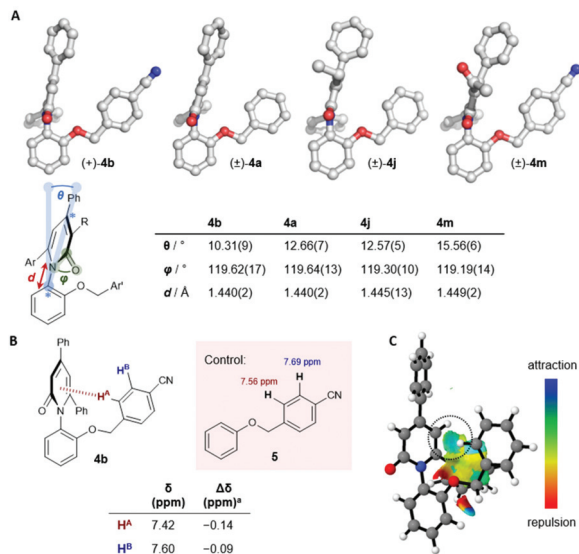


Fig. 2 A. Single crystal X-ray structures of (+)-**4b**, **4a**, **4j** and **4m** (CCDC 2124210, 2124211, 2124208 and 2124209† respectively). The values of φ and d and their standard uncertainties are obtained directly from the .cif file. The angle between the indicated atoms (*) was measured using Mercury¹⁴ and used to determine the value of θ . B. Comparison between selected ^1H NMR chemical shifts for **4b** and control **5**¹⁵ indicative of $\text{CH}\cdots\pi$ interaction. $\Delta\delta$ calculated as $\delta(\text{4b}) - \delta(\text{5})$. C. Non-Covalent Interaction (NCI) surface of the minimum of **4a** showing a stabilising $\text{CH}^{\text{A}}-\pi$ interaction in light blue (circled). The colour spectrum ranges from blue (strongly attractive) to green (weakly attractive) to yellow (mildly repulsive) to red (strongly repulsive), geometries optimised at B3LYP-D3/6-31G(d,p).

tilt is the formation of a $\text{CH}\cdots\pi$ interaction between the *ortho*-CH of the benzyl group and the π -system of the 2-pyridone.¹³ Aromatic C–H signals for the 4-cyanobenzyl group are shifted upfield by 0.14 (H^{A}) and 0.09 (H^{B}) ppm relative to the control,¹⁵ consistent with the upfield shifts observed by Jennings and Malone in related $\text{CH}\cdots\pi$ systems.¹⁶ This interaction has a stabilising influence on the ground state that is necessarily absent in the enantiomerisation transition state, increasing the overall barrier to racemisation. Rotational profiles of selected starting materials, deprotonated phenolate intermediates and products were examined by DFT (see ESI†). These calculations emphasise the importance of hydrogen bonding in this reaction manifold. The rotational barrier in the starting material is lowered through the transition state $\text{OH}\cdots\text{O}$ interaction, whilst the deprotonated intermediate lacking this stabilising interaction displays a significantly higher barrier. The product barrier is raised through the ground state $\text{CH}\cdots\pi$ stabilising interaction observed in the crystal structure, supported by ^1H chemical shift values, and replicated in solution phase calculations (Fig. 2C).

To understand the origin of asymmetric induction we attempted to co-crystallize the substrate (**3c**) anion with the catalyst (**C4**) cation (Fig. 3A). The only crystals obtained were of the desired ion pair, alongside a second neutral substrate molecule presumably formed through protonation by adventitious water during prolonged recrystallization (Fig. 3B). The proton acts as a bridge between the oxygen atoms, and it is likely irrelevant which phenol formally bears the negative charge since the proton is in rapid exchange. The importance of phenol-phenolate heterodimers in (achiral) PTC has previously been noted by Denmark,¹⁷ and for certain ammonium salt catalysts it has been suggested that the $[\text{PhO}-\text{H}\cdots\text{OPh}]^-$ heterodimer is directly involved in the $\text{S}_{\text{N}}2$ alkylation.¹⁸ Here, the proton-bridged phenolate dimer contains both the (*R_a*)- and (*S_a*)-configured biaryls, where the former corresponds to the major enantiomer formed in the catalytic reaction. The

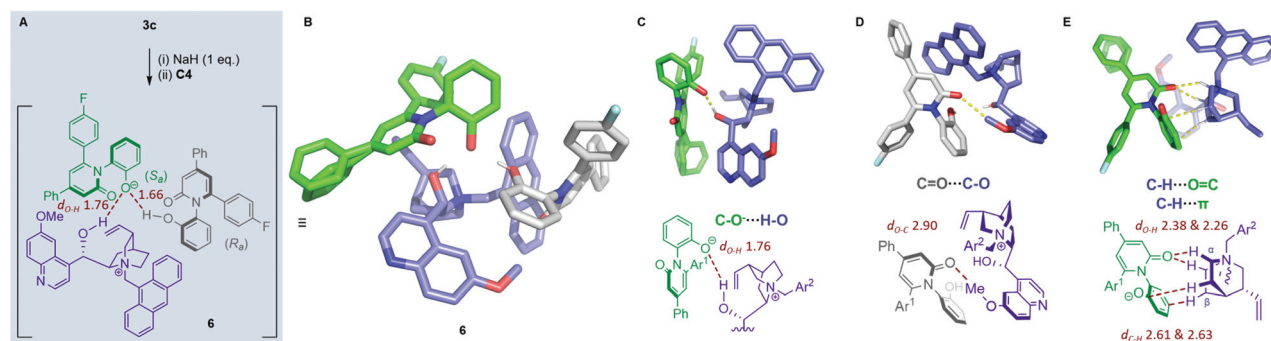


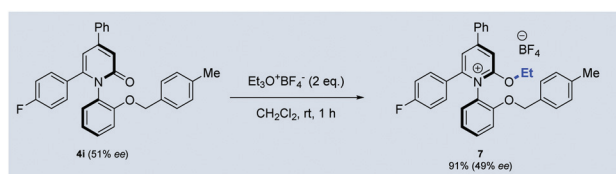
Fig. 3 (A) Synthesis of co-crystal **6**. **3c**-derived phenolate (in green), **C4** catalyst quaternary cation (in purple) and neutral phenol **3c** spectator (in grey). (B) Single crystal X-ray structure of ternary complex **6** (CCDC 2124143†).²⁰ The phenolate (in green) displays some disorder in the *para*-phenyl substituent. (C)–(E) The ensemble of intermolecular non-covalent interactions (dashed lines) displayed between the quinidinium cation and the neutral and anionic substrates. All contacts calculated to be shorter than the sum of VDW radii minus 0.2 Å are shown, except those directly between the neutral and anionic substrates. Bond lengths relevant to the non-covalent interactions are given (Å, in maroon). Species not involved in each interaction are omitted for clarity. In (E) the interaction occurs between a pyridone phenolate and quinolinium cation in adjacent asymmetric units, so this interaction is not visible in (B). Ar^1 = 4-fluorophenyl; Ar^2 = 9-anthracenyl.



complexity of this ternary structure precludes definitive statements regarding asymmetric induction. However, ground-state observations may aid the community in understanding how anionic intermediates bind to *cinchona*-derived ammonium salts.¹⁹ The following interactions are evident: (i) the phenoxide is engaged in a O–H...O hydrogen bond with the secondary alcohol of the catalyst (Fig. 3C). This interaction has previously been noted,^{19,21} and is evidently important for asymmetric induction since *O*-allyl catalyst **C2** gave much poorer enantioselectivity (see Table 1); (ii) a short contact between the pyridone C=O and the CH₃ of the catalyst suggests an n → σ* interaction (Fig. 3D), consistent with the “oxyanion hole” previously described by Wong;²² (iii) a series of two N⁺C_α–H...O and two C_β–H...π interactions acting in unison leading to a tetrapodal array (Fig. 3E). N⁺C_α–H...O interactions in asymmetric catalysis involving ammonium salts has been extensively discussed,²³ and the interaction we observe between these N⁺C_α–H donors and the pyridone carbonyl is reminiscent of those with DMF recently noted by Veticatt, Waser and Adamo.¹⁹ To our knowledge C_β–H interactions have not previously been proposed or observed for *cinchona* ammoniums, though Yamanaka and Shirakawa proposed a similar interaction in the optimized transition state for a tetraalkylammonium-catalysed aza-Diels–Alder reaction.²⁴ Knowledge of these myriad interactions may inform efforts to understand and optimize *cinchona* alkaloid-catalysed asymmetric PTC through theory²⁵ and experiment.²⁶

Our initial interest in asymmetric pyridone synthesis stemmed from work generating axially chiral *N*-aryl quinolinium salts. We sought to determine if an *N*-aryl pyridinium species could be formed from these 2-pyridones (**4**). Treatment of **4i** with Et₃O⁺BF₄[−] gave pyridinium tetrafluoroborate salt **7** in 91% yield, with a small reduction from 51% ee to 49% ee (Scheme 2). Since several enantioselective methods exist to generate 2-pyridones and related structures,^{1a–c} this constitutes a general method to generate axially chiral pyridinium cations and their congeners.

In summary, chiral PTC enabled the DKR of *N*-aryl pyridones generating C–N axially chiral products in good to poor ee, with a strong substrate dependence. The difference in rotational barriers between the starting material and product were probed by a combination of experiment and quantum chemical calculation, revealing crucial non-covalent O–H...O and C–H...π interactions lying at the heart of this reaction manifold. Important non-covalent interactions were also revealed in the substrate–catalyst complex through X-ray diffraction that may aid in understanding the behaviour of *cinchona*-derived ammonium catalysts in this and other reactions.



Scheme 2 Stereo-retentive synthesis of axially chiral pyridinium tetrafluoroborate salts.

action that may aid in understanding the behaviour of *cinchona*-derived ammonium catalysts in this and other reactions.

Conflicts of interest

There are no conflicts to declare.

Notes and references

- (a) J. K. Cheng, S. H. Xiang, S. Li, L. Ye and B. Tan, *Chem. Rev.*, 2021, **121**, 4805–4902; (b) E. Kumarasamy, R. Raghunathan, M. P. Sibi and J. Sivaguru, *Chem. Rev.*, 2015, **115**, 11239–11300; (c) I. Takahashi, Y. Suzuki and O. Kitagawa, *Org. Prep. Proced. Int.*, 2014, **46**, 1–23; (d) O. Kitagawa, *Acc. Chem. Res.*, 2021, **54**, 719–730; (e) J. S. Sweet and P. C. Knipe, *Synthesis*, 2022, DOI: 10.1055/s-0040-1719896.
- (a) X. Z. Fan, X. Zhang, C. Y. Li and Z. H. Gu, *ACS Catal.*, 2019, **9**, 2286–2291; (b) T. Hirata, I. Takahashi, Y. Suzuki, H. Yoshida, H. Hasegawa and O. Kitagawa, *J. Org. Chem.*, 2016, **81**, 318–323; (c) S. L. Li, C. Yang, Q. Wu, H. L. Zheng, X. Li and J. P. Cheng, *J. Am. Chem. Soc.*, 2018, **140**, 12836–12843; (d) Z.-S. Liu, P.-P. Xie, Y. Hua, C. Wu, Y. Ma, J. Chen, H.-G. Cheng, X. Hong and Q. Zhou, *Chem*, 2021, **7**, 1917–1932; (e) N. Man, Z. Lou, Y. Li, H. Yang, Y. Zhao and H. Fu, *Org. Lett.*, 2020, **22**, 6382–6387; (f) J. Y. Ong, X. Q. Ng, S. C. Lu and Y. Zhao, *Org. Lett.*, 2020, **22**, 6447–6451; (g) Y.-B. Wang, S.-C. Zheng, Y.-M. Hu and B. Tan, *Nat. Commun.*, 2017, **8**, 15489; (h) G.-H. Yang, H. Zheng, X. Li and J.-P. Cheng, *ACS Catal.*, 2020, **10**, 2324–2333; (i) D. Li, S. Wang, S. Ge, S. Dong and X. Feng, *Org. Lett.*, 2020, **22**, 5331–5336; (j) G. Zheng, X. Li and J.-P. Cheng, *Org. Lett.*, 2021, **23**, 3997–4001.
- (a) K. T. Barrett, A. J. Metrano, P. R. Rablen and S. J. Miller, *Nature*, 2014, **509**, 71–75; (b) K. T. Barrett and S. J. Miller, *J. Am. Chem. Soc.*, 2013, **135**, 2963–2966; (c) M. E. Diener, A. J. Metrano, S. Kusano and S. J. Miller, *J. Am. Chem. Soc.*, 2015, **137**, 12369–12377; (d) S. D. Vaidya, S. T. Toenjes, N. Yamamoto, S. M. Maddox and J. L. Gustafson, *J. Am. Chem. Soc.*, 2020, **142**, 2198–2203; (e) Q.-J. Yao, P.-P. Xie, Y.-J. Wu, Y.-L. Feng, M.-Y. Teng, X. Hong and B.-F. Shi, *J. Am. Chem. Soc.*, 2020, **142**, 18266–18276; (f) J. Zhang, Q. Xu, J. Wu, J. Fan and M. Xie, *Org. Lett.*, 2019, **21**, 6361–6365; (g) S. Zhang, Q.-J. Yao, G. Liao, X. Li, H. Li, H.-M. Chen, X. Hong and B.-F. Shi, *ACS Catal.*, 2019, **9**, 1956–1961.
- (a) N. Di Iorio, F. Champavert, A. Erice, P. Righi, A. Mazzanti and G. Bencivenni, *Tetrahedron*, 2016, **72**, 5191–5201; (b) N. Di Iorio, P. Righi, A. Mazzanti, M. Mancinelli, A. Cioagli and G. Bencivenni, *J. Am. Chem. Soc.*, 2014, **136**, 10250–10253; (c) N. Di Iorio, L. Soprani, S. Crotti, E. Marotta, A. Mazzanti, P. Righi and G. Bencivenni, *Synthesis*, 2017, **49**, 1519–1530; (d) H. C. Liu, H. Y. Tao, H. J. Cong and C. J. Wang, *J. Org. Chem.*, 2016, **81**, 3752–3760; (e) J. L. Zhang, Y. L. Zhang, L. L. Lin,



- Q. Yao, X. H. Liu and X. M. Feng, *Chem. Commun.*, 2015, **51**, 10554–10557; (f) J. W. Zhang, J. H. Xu, D. J. Cheng, C. Shi, X. Y. Liu and B. Tan, *Nat. Commun.*, 2016, **7**, 10677; (g) L. L. Zhang, J. W. Zhang, S. H. Xiang, Z. Guo and B. Tan, *Org. Lett.*, 2018, **20**, 6022–6026.
- 5 (a) M. Auge, A. Feraldi-Xypolia, M. Barbazanges, C. Aubert, L. Fensterbank, V. Gandon, E. Kolodziej and C. Ollivier, *Org. Lett.*, 2015, **17**, 3754–3757; (b) K. Tanaka, Y. Takahashi, T. Suda and M. Hirano, *Synlett*, 2008, 1724–1728, DOI: 10.1055/s-2008-1078488.
- 6 (a) H.-Y. Bai, F.-X. Tan, T.-Q. Liu, G.-D. Zhu, J.-M. Tian, T.-M. Ding, Z.-M. Chen and S.-Y. Zhang, *Nat. Commun.*, 2019, **10**, 3063; (b) J. Frey, S. Choppin, F. Colobert and J. Wencel-Delord, *Chimia*, 2020, **74**, 883–889; (c) J. Frey, A. Malekafzali, I. Delso, S. Choppin, F. Colobert and J. Wencel-Delord, *Angew. Chem., Int. Ed.*, 2020, **59**, 8844–8848; (d) Q. Ren, T. Cao, C. He, M. Yang, H. Liu and L. Wang, *ACS Catal.*, 2021, **11**, 6135–6140; (e) V. Thonnissen and F. W. Patureau, *Chem. – Eur. J.*, 2021, **27**, 7189–7192; (f) S. Brandes, M. Bella, A. Kjærsgaard and K. A. Jørgensen, *Angew. Chem., Int. Ed.*, 2006, **45**, 1147–1151.
- 7 J. S. Sweet, S. Rajkumar, P. Dingwall and P. C. Knipe, *Eur. J. Org. Chem.*, 2021, 3980–3985.
- 8 A. J. Fugard, A. S. K. Lahdenpera, J. S. J. Tan, A. Mekareeya, R. S. Paton and M. D. Smith, *Angew. Chem., Int. Ed.*, 2019, **58**, 2795–2798.
- 9 B. E. Dial, P. J. Pellechia, M. D. Smith and K. D. Shimizu, *J. Am. Chem. Soc.*, 2012, **134**, 3675–3678.
- 10 J. A. Carmona, C. Rodríguez-Franco, R. Fernández, V. Hornillos and J. M. Lassaletta, *Chem. Soc. Rev.*, 2021, **50**, 2968–2983.
- 11 Q.-H. Teng, X.-J. Peng, Z.-Y. Mo, Y.-L. Xu, H.-T. Tang, H.-S. Wang, H.-B. Sun and Y.-M. Pan, *Green Chem.*, 2018, **20**, 2007–2012.
- 12 C. Wolf, D. H. Hochmuth, W. A. König and C. Roussel, *Liebigs Ann.*, 1996, **1996**, 357–363.
- 13 M. Nishio and M. Hirota, *Tetrahedron*, 1989, **45**, 7201–7245.
- 14 C. F. Macrae, I. Sovago, S. J. Cottrell, P. T. A. Galek, P. McCabe, E. Pidcock, M. Platings, G. P. Shields, J. S. Stevens, M. Towler and P. A. Wood, *J. Appl. Crystallogr.*, 2020, **53**, 226–235.
- 15 G. A. Molander and B. Canturk, *Org. Lett.*, 2008, **10**, 2135–2138.
- 16 W. B. Jennings, B. M. Farrell and J. F. Malone, *Acc. Chem. Res.*, 2001, **34**, 885–894.
- 17 S. E. Denmark, R. C. Weintraub and N. D. Gould, *J. Am. Chem. Soc.*, 2012, **134**, 13415–13429.
- 18 I. C. Nogueira and J. R. Pliego, *Mol. Catal.*, 2021, **506**, 111566.
- 19 G. Bencivenni, D. Salazar Illera, M. Moccia, K. N. Houk, J. A. Izzo, J. Novacek, P. Grieco, M. J. Veticatt, M. Waser and M. F. A. Adamo, *Chem. – Eur. J.*, 2021, **27**, 11352–11366.
- 20 We thank the EPSRC UK National Crystallography Service at the University of Southampton for the collection of the crystallographic data. S. J. Coles and P. A. Gale, *Chem. Sci.*, 2012, **3**, 683–689.
- 21 U. H. Dolling, P. Davis and E. J. J. Grabowski, *J. Am. Chem. Soc.*, 1984, **106**, 446–447.
- 22 H. Yang and M. W. Wong, *J. Am. Chem. Soc.*, 2013, **135**, 5808–5818.
- 23 (a) C. E. Cannizzaro and K. N. Houk, *J. Am. Chem. Soc.*, 2002, **124**, 7163–7169; (b) T. Nakamura, K. Okuno, R. Nishiyori and S. Shirakawa, *Chem. – Asian J.*, 2020, **15**, 463–472; (c) M. Yasui, A. Yamada, C. Tsukano, A. Hamza, I. Pápai and Y. Takemoto, *Angew. Chem., Int. Ed.*, 2020, **59**, 13479–13483.
- 24 M. Yamanaka, A. Mochizuki, T. Nakamura, K. Maruoka and S. Shirakawa, *Heterocycles*, 2020, **101**, 580–592.
- 25 (a) C. Q. He, A. Simon, Y.-H. Lam, A. P. J. Brunskill, N. Yasuda, J. Tan, A. M. Hyde, E. C. Sherer and K. N. Houk, *J. Org. Chem.*, 2017, **82**, 8645–8650; (b) J. R. Pliego, *Org. Biomol. Chem.*, 2021, **19**, 1900–1914; (c) E. De Freitas Martins and J. R. Pliego, *ACS Catal.*, 2013, **3**, 613–616; (d) E. F. Martins and J. R. Pliego, *J. Mol. Catal. A: Chem.*, 2016, **417**, 192–199.
- 26 (a) S. E. Denmark and R. C. Weintraub, *Heterocycles*, 2010, **82**, 1527–1540; (b) K. W. Lexa, K. M. Belyk, J. Henle, B. Xiang, R. P. Sheridan, S. E. Denmark, R. T. Ruck and E. C. Sherer, *Org. Process Res. Dev.*, 2021, DOI: 10.1021/acs.oprd.1c00155.

